



Multiwavelength Quasi-periodic Pulsations in a Stellar Superflare

Dmitrii Y. Kolotkov^{1,2} , Valery M. Nakariakov^{1,3} , Robin Holt¹, and Alexey A. Kuznetsov²

¹ Centre for Fusion, Space and Astrophysics, Department of Physics, University of Warwick, CV4 7AL, UK; D.Kolotkov.1@warwick.ac.uk

² Institute of Solar-Terrestrial Physics, Irkutsk 664033, Russia

³ St. Petersburg Branch, Special Astrophysical Observatory, Russian Academy of Sciences, 196140, St. Petersburg, Russia

Received 2021 November 18; revised 2021 December 12; accepted 2021 December 14; published 2021 December 24

Abstract

We present the first multiwavelength simultaneous detection of quasi-periodic pulsations (QPPs) in a superflare (more than a thousand times stronger than known solar flares) on a cool star, in soft X-rays (SXRs, with XMM-Newton) and white light (WL, with Kepler). It allowed for the first ever analysis of oscillatory processes in a stellar flare simultaneously in thermal and nonthermal emissions, conventionally considered to come from the corona and chromosphere of the star, respectively. The observed QPPs have periods 1.5 ± 0.15 hr (SXR) and 3 ± 0.6 hr (WL), and correlate well with each other. The unique relationship between the observed parameters of QPPs in SXR and WL allowed us to link them with oscillations of the electric current in the flare loop, which directly affect the dynamics of nonthermal electrons and indirectly (via ohmic heating) the thermal plasma. These findings could be considered in favor of the equivalent LCR contour model of a flare loop, at least in the extreme conditions of a stellar superflare.

Unified Astronomy Thesaurus concepts: Optical flares (1166); Stellar x-ray flares (1637); Stellar coronae (305); Stellar oscillations (1617); Solar oscillations (1515); Solar coronal waves (1995); Magnetohydrodynamics (1964)

1. Introduction

Solar flares and coronal mass ejections are the most powerful physical phenomena in the solar system, and the key driver of space weather (Schrijver 2011; Benz 2017). Physical processes operating in flaring sites, such as magnetic reconnection, charged particle acceleration, and turbulence remain key challenges of plasma astrophysics (e.g., Shibata & Magara 2011). The parametric range of the flare research is significantly broadened by observing flares on other stars, including those of solar type. In particular, observations of stellar superflares, with released energy several orders of magnitude higher than in the most energetic observed solar flare (e.g., Maehara et al. 2012) are important for assessing whether the Sun is capable of producing a devastating solar superflare.

Despite a tremendous effort in understanding the physics of flares, revealing a comprehensive generic model of a flare, consistent with observations remains one of the longest-standing and impactful questions for space weather research. In particular, the so-called *standard* model of a solar flare (Shibata & Magara 2011), based on a magnetohydrodynamic (MHD) description of the processes of current-sheet development, magnetic-field restructuring, and subsequent acceleration of charged particles, captures well the global picture of a flare, but struggles to explain more specific questions such as what triggers the flare, how the released energy is split between different channels (including manifestations in specific electromagnetic bands), and what determines the characteristic timescales. Considering the inductive property of solar atmospheric plasma configurations (i.e., the induction of the magnetic field by electric current systems and vice versa) as a fundamental storage of free magnetic energy, Alfvén &

Carlqvist (1967) proposed a flare model based on the analogy with a closed electric circuit. In this model, the disruption of the electric current leads to the explosive release of the whole magnetic energy of the circuit via local ohmic heating (cf. switches in high-power transmission networks).

An intriguing process not predicted by the standard flare model but commonly observed in solar flares are quasi-periodic pulsations (QPPs) of the emitted radiation, which have been detected in all spectral bands (see, e.g., Nakariakov & Melnikov 2009; Kupriyanova et al. 2020). Typically, QPPs appear as subsequent increases and decreases in the emission intensity, usually lasting for several cycles only. Often, oscillatory patterns in QPPs are nonstationary, i.e., are subject to amplitude and period modulations (see, e.g., Nakariakov et al. 2019). Physical mechanisms responsible for QPP are subject to intensive ongoing studies. It is expected that these mechanisms could be divided into three main groups: the modulation of the emitting plasma by MHD oscillations, repetitive magnetic reconnection which is periodically induced by an MHD oscillation, and spontaneous repetitive reconnection (see McLaughlin et al. 2018, for a comprehensive review). Taking the effective inductance (L), capacitance (C), and resistance (R) of coronal plasma configurations into account in the Alfvén's flare model (Alfvén & Carlqvist 1967), oscillatory variations of the electric current in the flare loop (considered as an equivalent LCR contour) were theoretically predicted as a unique feature of the model, naturally leading to QPPs (Zaitsev et al. 1998; Khodachenko et al. 2009; Zimovets et al. 2021). In general, the identification of the mechanism for a QPP requires simultaneous observations at different wavelengths which are associated with thermal and nonthermal emission, i.e., in different spectral bands, providing crucial information about the release and transport of flare energy through different layers of the solar atmosphere (Zimovets et al. 2021). In other words, no contemporary flare model is acceptable unless it adequately accounts for the phenomenon of QPPs.



Original content from this work may be used under the terms of the [Creative Commons Attribution 4.0 licence](#). Any further distribution of this work must maintain attribution to the author(s) and the title of the work, journal citation and DOI.

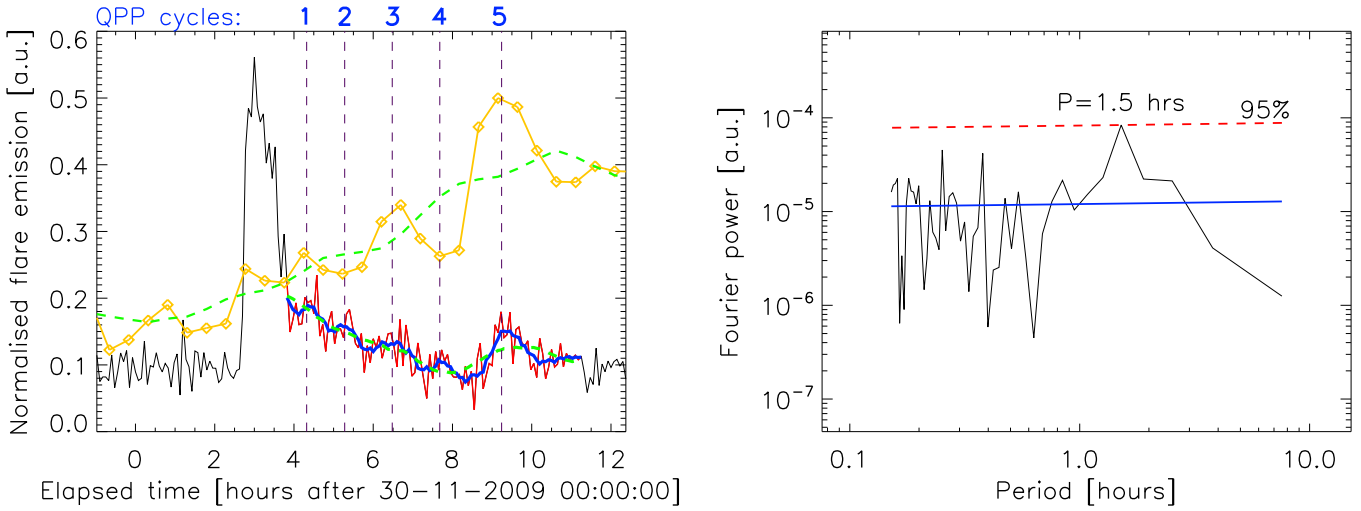


Figure 1. Left: normalized lightcurves of a superflare event, analyzed in this work, as seen by XMM-Newton in the soft X-ray band (SXR, the black–red solid curve) and by Kepler in the white light band (WL, the yellow line). The gradual trend of the WL lightcurve is caused by the background WL irradiance modulated by the star’s rotation (with a period of 6.043 days, see Section 2). The red curve shows the SXR signal in the time interval of interest, during which signatures of QPPs are detected. The green dashed lines show the long-term trends of the WL and SXR signals. The blue solid line shows the SXR signal’s interval of interest smoothed over 30 minutes, thus mimicking the time resolution of the WL lightcurve (used in Figure 3). Both lightcurves are normalized to some arbitrary constants for better visualization. Right: the Fourier power spectrum of the SXR signal of interest shown in red in the left-hand panel with the corresponding long-term trend subtracted. The blue solid line shows the best-fit of the spectrum by a power-law function. The red dashed line indicates the statistical significance level of 95%, estimated as described in Section 3.

QPPs are detected in stellar flares too, including the radio (e.g., Stepanov et al. 2001), soft X-rays (SXRs) (e.g., Mitrakraev et al. 2005), UV (e.g., Doyle et al. 2018), and white light (WL) (e.g., Pugh et al. 2016) bands. Empirical properties of QPPs in solar and stellar flares have similarities (Cho et al. 2016), which could indicate an analogy in their underlying physical processes. In particular, QPPs in stellar flares have been detected at different wavelengths within the same spectral band: in optics (Zhilyaev et al. 2000), in radio (Stepanov et al. 2001), and in SXR (Broomhall et al. 2019a). Guarcello et al. (2019) analyzed simultaneous observations of stellar superflares in the WL (with Kepler) and SXR (with XMM-Newton), and found 500 s QPPs in an SXR flare lightcurve on the M2 class star HCG 273. However, the corresponding periodicity was not revealed in the WL band. Thus, to the best of our knowledge there have been no simultaneous observations of QPPs in stellar superflares in distinctly different electromagnetic wave bands which would allow for distinguishing between thermal and nonthermal flare emissions so far.

The omnipresence of various transient wave and oscillatory phenomena in elastic media such as solar and stellar atmospheres naturally allows for the use of them as a unique tool for seismological diagnostics of the local plasma conditions and processes, which could not be measured otherwise. The successful application and potential of this approach has been confidently demonstrated for studying the local plasma conditions in the corona of the Sun known as coronal MHD seismology (see Nakariakov & Kolotkov 2020, for the most recent review), for which direct spatially and temporally resolved observations of MHD waves and oscillations are ubiquitously available. For stars, in the absence of direct spatially resolved observations, the only proxy of wave dynamics in their atmospheres is time-resolved observations of QPPs in the lightcurves of stellar flares and superflares. In other words, the phenomenon of QPPs offers a unique yet unexplored source of information about ongoing processes and physical conditions in the atmospheres of stars, through the

transfer of the method of MHD coronal seismology from solar physics to the realm of stellar physics and exploitation of the solar–stellar analogy. Such a promising perspective of a QPP-based stellar MHD coronal seismology clearly justifies the interest and high demand in multiwavelength observations of QPPs in stellar flares in distinctly different spectral bands. This would enable, in particular, studies of the development of flare energy releases at different layers of stellar atmospheres, and allow for advancing of our understanding of the physics of flares and the solar–stellar analogy in general.

In this Letter, we present the first ever detection of QPP signals in a stellar superflare simultaneously in the SXR and WL bands, typically associated with thermal and nonthermal emissions from the corona and chromosphere of the star, respectively. We identify a specific relationship between the observed WL and SXR QPP parameters (ratio of the oscillation periods), which could be interpreted as a plausible feature of the equivalent LCR contour oscillations in a stellar superflare (among at least 15 physical mechanisms/models that have been proposed to explain QPPs in flares; see McLaughlin et al. 2018; Kupriyanova et al. 2020; Zimovets et al. 2021).

2. Observations

We use simultaneous observations of a superflare that occurred on 2009 November 30 on the M3V class star KIC 8093473, obtained in the white light (WL) and SXR bands with the Kepler and XMM-Newton (0.2–12 keV, with the EPIC PN detector) missions, respectively (see the left-hand panel in Figure 1). By the peak X-ray flux, the analyzed stellar superflare was previously shown to be equivalent to X14,700 GOES-class solar flare (Kuznetsov & Kolotkov 2021; cf. the strongest X28-class solar flare ever observed). The analyzed flare was selected by inspecting the Kepler (Borucki et al. 2010) and XMM-Newton (Jansen et al. 2001; Rosen et al. 2016) databases. More specifically, among 69 stars observed simultaneously by both instruments (Pizzocaro et al. 2019), Kuznetsov & Kolotkov (2021) identified three stars with

several flares (some of which likely consisting of multiple emission peaks) manifesting simultaneously in the WL and X-ray bands. We study the presence of QPPs in one of those complex flaring events; the visual inspection of the lightcurves of other flares did not show signatures of quasi-periodic variability and therefore they are not discussed here.

The host star is considered to be a young, tidally locked binary consisting of two more or less similar red dwarfs (Kuznetsov & Kolotkov 2021), with orbital and rotation periods of 6.043 days (McQuillan et al. 2014) and a temperature of 3400 K (Gaia Collaboration 2018), at a distance of 206 pc (Gaia Collaboration 2018); the analyzed flare likely occurred on one of the components of the binary rather than in the interstellar space (Kuznetsov & Kolotkov 2021). The flare showed a rapid increase in the SXR flux, developing into a well-pronounced flare peak followed by several weaker quasi-periodic peaks in the flare-decay phase. In the WL observations, the event is manifested as a series of consecutive quasi-periodic peaks superposed on the background stellar irradiance modulated by the rotation period.

The WL observations by Kepler have a time cadence of 29.5 minutes, i.e., the Kepler data represent the WL flux binned (averaged) over this time interval. The SXR observations from XMM-Newton used in this work have a bin size (effective cadence) of 4.5 minutes. Based on the solar–stellar analogy, the emission mechanism for the WL radiation in flares is associated with the blackbody radiation from lower layers of the stellar atmosphere, heated by nonthermal electrons (Benz & Güdel 2010). In turn, the emission mechanism for the SXR radiation is associated with thermal radiation from a hot (~ 30 MK) coronal plasma (Güdel 2004). Earlier, Kuznetsov & Kolotkov (2021) rigorously demonstrated that the largest SXR flare peak in the analyzed flare is delayed with respect to its WL counterpart by 15 ± 23 minutes (with the uncertainty determined mainly by the time resolution of Kepler), which suggests the presence of the Neupert effect (Neupert 1968) as a characteristic signature of flare thermal and nonthermal emissions. In addition, the ratio of the WL to X-ray peak amplitudes was found to increase gradually with time, which was interpreted as a manifestation of the soft–hard–harder evolution of nonthermal electrons in the flare (see, e.g., Fletcher et al. 2011). At the same time, we would note that, despite being very common and apparently present in the considered event, the Neupert effect is not observed in all solar and stellar flares.

3. QPP Detection and Analysis

As the phenomenon of QPPs is traditionally distinguished from the flux variability caused by the flare itself (see, e.g., Cho et al. 2016), for the detection of QPPs in this work, we focus on the decay phase of the SXR flare lightcurve, i.e., after the main flare peak (see the interval of interest shown in red in the left-hand panel of Figure 1). Likewise, we use the Fourier-transform-based method complemented by a rigorous assessment of the statistical significance of the obtained Fourier components in comparison with a power-law distributed noisy background (Vaughan 2005; Pugh et al. 2017) as the most robust and straightforward approach for detection of QPPs in solar and stellar flares (Broomhall et al. 2019b). A slowly varying trend of the original signal, $T_{\text{SXR}}(t)$ is subtracted before applying the Fourier analysis. In this work, the SXR trend is obtained by smoothing the original signal over 150 minutes,

using a Savitzky–Golay polynomial filter. Having assessed the presence of QPPs in the SXR flare lightcurve, we calculate the SXR modulation depth as $\delta F_{\text{SXR}}(t) = [F_{\text{SXR}}(t) - T_{\text{SXR}}(t)]/T_{\text{SXR}}(t)$.

For the WL emission, we obtain a slowly varying trend $T_{\text{WL}}(t)$ by smoothing the original signal over 265 minutes, which gives the modulation depth $\delta F_{\text{WL}}(t) = [F_{\text{WL}}(t) - T_{\text{WL}}(t)]/T_{\text{WL}}(t)$. Due to low time resolution of the WL signal, we assess the presence of quasi-periodic behavior in it via cross correlating $\delta F_{\text{WL}}(t)$ with $\delta F_{\text{SXR}}(t)$ and $[\delta F_{\text{WL}}(t)]^2$ with $\delta F_{\text{SXR}}(t)$.

For checking the cross correlation between the latter, i.e., $[\delta F_{\text{WL}}(t)]^2$ and $\delta F_{\text{SXR}}(t)$, we represent $\delta F_{\text{WL}}(t)$ as $\delta F_{\text{WL}}(t) = A_0(t)\cos\omega t$ where ω and $A_0(t)$ are the characteristic oscillation frequency and instantaneous amplitude determined as

$$A_0(t) = |\delta F_{\text{WL}}(t) + i\mathcal{H}\{\delta F_{\text{WL}}(t)\}|, \quad (1)$$

where $\mathcal{H}\{\delta F_{\text{WL}}(t)\}$ is the Hilbert transform of $\delta F_{\text{WL}}(t)$ (Huang et al. 1998). Applying the trigonometric identity $\cos^2\alpha = (1 + \cos 2\alpha)/2$, $\delta F_{\text{WL}}^2(t)$ can be rewritten as $\delta F_{\text{WL}}^2(t) = A_0^2(t)[1 + \cos 2\omega t]/2$. From here, we isolate $\tilde{\delta F}_{\text{WL}}^2(t) \equiv A_0(t)\cos 2\omega t$ which becomes

$$\tilde{\delta F}_{\text{WL}}^2(t) = \frac{2[\delta F_{\text{WL}}(t)]^2 - A_0^2(t)}{A_0(t)}. \quad (2)$$

The new signal $\tilde{\delta F}_{\text{WL}}^2(t)$ takes into account a nonstationary oscillation amplitude $A_0(t)$ of the input signal $\delta F_{\text{WL}}(t)$ and has approximately zero mean, which allows for direct comparison of $\tilde{\delta F}_{\text{WL}}^2(t)$ with $\delta F_{\text{SXR}}(t)$ (see the right-hand panel in Figure 2).

4. Results

The Fourier power spectrum in Figure 1 clearly shows the presence of QPPs with a period of about 1.5 hr in the detrended SXR flux in the decay phase of the flare, composed of 5 well-pronounced oscillation cycles in the time domain (see the left-hand panel of Figure 1).

The star’s WL emission during the time interval of interest, for which QPPs are detected in SXR, also exhibits a quasi-periodic variation of intensity. Moreover, the QPP cycles 1, 3, 5 (2, 4) in the SXR band are seen to be in-phase (anti-phase) with the WL pulsations. The observed tendency strongly suggests that the period of modulation of the WL emission is two times longer than that in the SXR signal, thus being about 3 hr. This observational finding provides the first ever simultaneous detection of QPP signatures in a stellar superflare in two distinctly different wave bands, which could be associated with thermal and nonthermal emission mechanisms and their comparative analysis.

As there are only a few peaks with a few data points per period for both WL and SXR signals, we assess the uncertainties in the WL and SXR period measurements, $P_{\text{WL}} \pm \Delta_{\text{WL}}$ and $P_{\text{SXR}} \pm \Delta_{\text{SXR}}$ by a half width of the FFT frequency bin for the considered duration of the time interval of interest, $\Delta f \approx 0.07 \text{ hr}^{-1}$. Using this, Δ_{WL} and Δ_{SXR} can be estimated as $\Delta_{\text{WL}} = P_{\text{WL}}^2 \Delta f$ and $\Delta_{\text{SXR}} = P_{\text{SXR}}^2 \Delta f$, which gives $P_{\text{SXR}} = 1.5 \pm 0.15$ hr and $P_{\text{WL}} = 3 \pm 0.6$ hr. The uncertainty in the period ratio $P_{\text{WL}}/P_{\text{SXR}}$ then becomes $(P_{\text{WL}}/P_{\text{SXR}}) \sqrt{(\Delta_{\text{WL}}/P_{\text{WL}})^2 + (\Delta_{\text{SXR}}/P_{\text{SXR}})^2}$, which gives $P_{\text{WL}}/P_{\text{SXR}} = 2 \pm 0.4$.

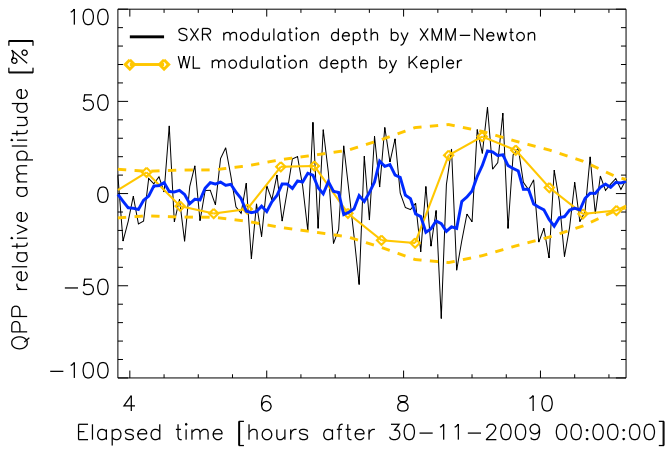


Figure 2. Left: the modulation depth, which is the ratio of the detrended original flare lightcurve to its long-term trend, of QPPs observed in the SXR band, $\delta F_{\text{SXR}}(t)$, and in the WL band, $\delta F_{\text{WL}}(t)$. The blue solid line is analogous to that shown in Figure 1. The yellow dashed lines show the instantaneous amplitude of $\delta F_{\text{WL}}(t)$, obtained by Equation (1). Right: the SXR modulation depth $\delta F_{\text{SXR}}(t)$ (the same as shown in the left-hand panel) and a normalized square of the WL modulation depth $\delta \tilde{F}_{\text{WL}}^2(t)$ determined by Equation (2).

The doubling of the QPP period in the WL signal, detected for the original flare lightcurves (Figure 1), is also evident in Figure 2 from comparison of the time history of the corresponding modulation depth signals, $\delta F_{\text{SXR}}(t)$ and $\delta F_{\text{WL}}(t)$. To perform a rigorous cross correlation analysis between the oscillatory patterns seen in SXR and WL, we use $\delta \tilde{F}_{\text{WL}}^2(t)$ given by Equation (2) and $\delta F_{\text{SXR}}(t)$. The results of the cross correlation analysis between $\delta \tilde{F}_{\text{WL}}^2(t)$ and $\delta F_{\text{SXR}}(t)$ are shown in Figure 3, demonstrating the highest value of the cross correlation coefficient reaches 0.5 at zero time lag. We note that this estimate of the cross correlation coefficient is strongly affected by noise present in the SXR observations. However, if we smooth the SXR signal over 30 minutes, thus effectively reproducing the time resolution of Kepler observations, the value of the cross correlation coefficient between $\delta \tilde{F}_{\text{WL}}^2(t)$ and $\delta F_{\text{SXR}}(t)$ at zero time lag increases to 0.82. The latter rigorously confirms strong correlation between the analyzed multiband stellar QPP signals and supports the conclusion that the QPP oscillation period observed in WL is two times longer than that in SXR.

To demonstrate that the observed correlation between the WL and SXR signals is not of a random nature, we performed the Fisher randomization test (see, e.g., Chorley et al. 2010, for the application of Fisher randomization to oscillations in sunspots). Our test implies the estimation of the probability of obtaining the cross correlation coefficient between $\delta \tilde{F}_{\text{WL}}^2(t)$ and $\delta F_{\text{SXR}}(t)$ higher than 0.8 (at any time lag) after a random permutation of the data points in $\delta \tilde{F}_{\text{WL}}^2(t)$. We found that the cross correlation >0.8 appears in less than 1% of all 10^6 random permutations considered, which indicates in favor of a nonrandom nature of the observed high correlation between QPP signals in WL and SXR with the confidence exceeding 99%.

5. Discussion

The analysis reveals that QPPs are present in both SXR and WL bands, with the oscillation periods 1.5 ± 0.15 hr and 3 ± 0.6 hr, respectively. These periods are much shorter than the stellar rotation period (~ 6 days) and hence the observed oscillations cannot be attributed to the effect of rotational modulation (see the events presented by Ilin et al. 2021).

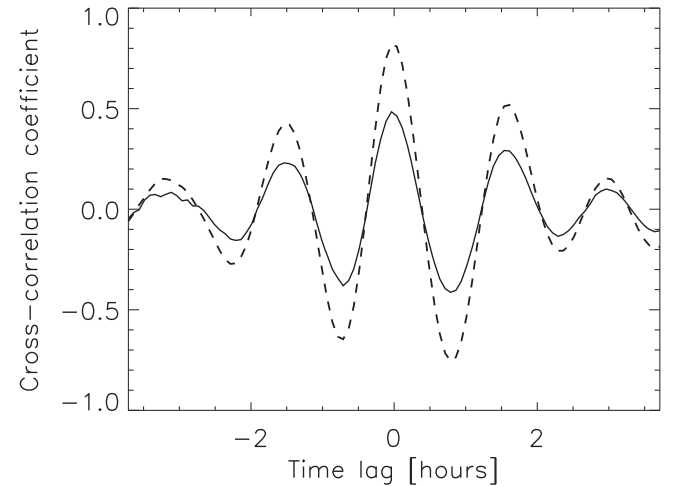
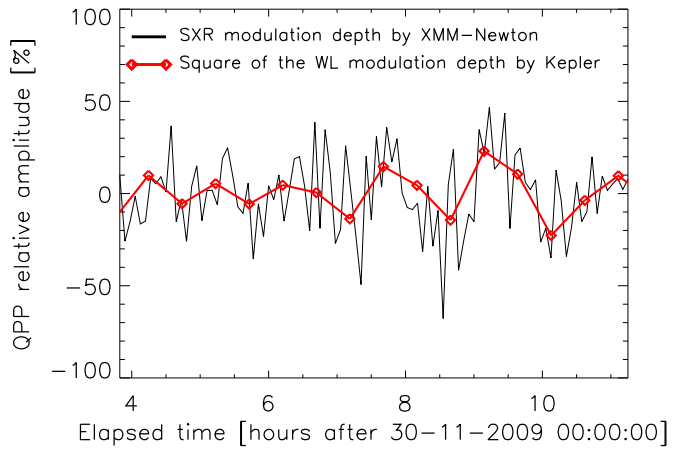


Figure 3. Results of the cross correlation analysis between the SXR modulation depth $\delta F_{\text{SXR}}(t)$ and the normalized square of the WL modulation depth $\delta \tilde{F}_{\text{WL}}^2(t)$. The solid and dashed curves show the cross correlation coefficients for the original $\delta \tilde{F}_{\text{WL}}^2(t)$ and original $\delta F_{\text{SXR}}(t)$, shown in the right-hand panel of Figure 2, and for the original $\delta \tilde{F}_{\text{WL}}^2(t)$ and $\delta F_{\text{SXR}}(t)$ smoothed over 30 minutes (thus effectively mimicking the time resolution of the WL signal; see Figures 1 and 2), respectively.

Likewise, the detection of similar QPP patterns in multi-instrumental independent observations is, in general, a strong indication of their stellar origin (see, e.g., Inglis et al. 2011). By the order of magnitude, the oscillation periods of WL QPP are consistent with the values detected in WL on other stars by, e.g., Anfinogentov et al. (2013) and Pugh et al. (2015, 2016). However, for the first time, a similar QPP pattern is simultaneously detected in SXR too. Moreover, the WL QPP has an oscillation period two times longer than the SXR QPPs. This finding provides us with crucial information for revealing the mechanism responsible for the oscillatory modulation of the emissions. In the following, we assume the widely accepted association of the SXR emission with the thermal emission from the flaring coronal loop (Güdel 2004) and the WL emission with nonthermal emission from the loop's footpoints (Benz & Güdel 2010).

Despite the variety of known mechanisms that could produce QPP (McLaughlin et al. 2018; Zimovets et al. 2021), it is

nontrivial to identify one that would explain why the SXR emission has an oscillation period two times shorter than that of the WL emission. One possible option is that the flaring loop experiences the second parallel harmonic of the sausage oscillation (e.g., Li et al. 2020). The periodic narrowing of the magnetic flux tube that forms the coronal part of the loop, occurs alternatively in the opposite legs of the loop, causing the periodic precipitation of nonthermal electrons in the alternate footpoints due to periodically varying magnetic mirror ratio (Nakariakov & Melnikov 2009). As the characteristic loop length is comparable to the radius of the star (Kuznetsov & Kolotkov 2021), it is likely that only one footpoint appears to be on the visible hemisphere of the star. Thus, $F_{WL}(t)$ comes from this footpoint only, with the oscillation period of the sausage mode, while $F_{SXR}(t)$ comes from the coronal part with the oscillation period two times shorter. Sausage oscillation periods are

$$P_{\text{saus}} \approx \frac{\pi r_{\min}}{2.4 C_{A0}}, \quad (3)$$

determined by the minor radius of the loop, r_{\min} and the Alfvén speed C_{A0} inside it (Nakariakov et al. 2012). For $r_{\min} \approx 5$ Mm and $C_{A0} \approx 500$ km s⁻¹, typical for solar flares, $P_{\text{saus}} \approx 10$ s. For the periods of 10⁴ s observed in this work, either r_{\min} should be 1000 times larger than in the solar case, or 100 times larger with the Alfvén speed 10 times lower than in the solar case. Since the required radius of the magnetic loop, even for the lowest reasonable Alfvén speeds, becomes comparable to the loop length and the stellar radius, this explanation is unlikely.

Another possible interpretation of the observed QPP is provided by the equivalent LCR contour model (Zaitsev et al. 1998; Zaitsev & Stepanov 2008; Khodachenko et al. 2009). In this model, the flaring active region is considered as a closed electric circuit (Alfvén & Carlqvist 1967). In the fully ionized coronal part, the electric current is guided by the loop-like magnetic field. In the partly ionized photosphere, the current can go across the field between the footpoints of the loop, closing the circuit. Such an electric circuit has a capacitance, inductance, and resistance determined by parameters of the plasma loop. Thus, the alternate electric current may experience oscillations with the period

$$P_{\text{LCR}} \approx \frac{(2\pi)^{3/2} \Lambda^{1/2} r_{\min}^2 \rho_0^{1/2} c}{I_0} \left(1 + \frac{c^2 r_{\min}^2 B_{||0}^2}{4I_0^2} \right)^{-1/2}, \quad (4)$$

where ρ_0 , I_0 and $B_{||0}$ are the mass density, and the electric current and parallel magnetic field in the loop in the equilibrium, respectively; c is the speed of light; and $\Lambda = \ln \frac{4L}{\pi r_{\min}} - 7/4$, with L being the loop length (see, e.g., Khodachenko et al. 2009; Tan et al. 2016). For $L = 700$ Mm, $r_{\min} = 30$ Mm, $\rho_0 = 3 \times 10^{-12}$ g cm⁻³, $B_{||0} = 30$ G, typical for stellar coronae (see, e.g., Monsignori Fossi et al. 1996; Mitra-Kraev et al. 2005; Mathioudakis et al. 2006; Kuznetsov & Kolotkov 2021; Ramsay et al. 2021), and a broad range of electric currents $I_0 = 10^8$ – 10^{12} A (see, e.g., Khodachenko et al. 2009), we obtain P about 10⁴ s. This value is consistent with the observed period. The damping of such oscillations has been estimated to be rather weak (Zaitsev et al. 1998), which is consistent with the observed behavior too. In this scenario, the thermal emission from the coronal loop could be caused by the

ohmic dissipation of the current I , i.e., $F_{SXR}(t) \propto I^2(t)$. Taking that $I(t) = I_0 + \tilde{I}(t)$, where \tilde{I} is the oscillating alternate current, we conclude that F_{SXR} oscillates with double the period of $\tilde{I}(t)$ if the amplitude of \tilde{I} is greater than I_0 .

The presented results could be considered in favor of the equivalent LCR contour nature of stellar flare loops. To the best of our knowledge, in the multitude of QPP models proposed hitherto (Zimovets et al. 2021), there are no other mechanisms that could simultaneously (a) cause modulation of thermal and nonthermal flare emissions, (b) give observed periods of 10⁴ s for reasonable combinations of stellar flare conditions, and (c) explain the observed ratio of thermal and nonthermal QPP periods. The simultaneous oscillations in the thermal (SXR) and nonthermal (WL) emissions, and hence their similarities or differences, are hard to study in solar flares, for which the WL emission is rare and usually short-lived (Benz 2017). However, extreme physical conditions in far more powerful stellar superflares make it possible to detect the WL emission co-existing with the SXR emission for a sufficiently long time, and to study oscillatory processes superimposed. Results obtained in this Letter open up a new opportunity for exploiting the analogy between solar and stellar flares via searching for similar correlations between oscillations in thermal and nonthermal flare emissions from the Sun, by using observations from existing and future high-resolution and high-sensitivity instruments.

The intrinsic difficulties preventing the direct comparison and extrapolation of the results obtained in our work to solar flares are the lack of general understanding of differences and/or similarities between physics of WL flares on the Sun and other stars (Benz & Güdel 2010) and the huge disparity in physical conditions and characteristic spatial and temporal scales in solar and stellar flares, which might lead to different observational manifestations of the same quasi-periodic modulation process. One of the illustrations of these difficulties is the lack of observations of QPP in WL solar flares.

Our work suggests that the QPP period ratio of two in thermal and nonthermal emissions could be indicative of the operation of the LCR mechanism, at least in the extreme conditions of stellar superflares. However, the LCR model is not an exclusive mechanism for simultaneous QPPs in thermal and nonthermal emissions. Indeed, there are at least several other physical mechanisms that could cause quasi-periodic modulation simultaneously in thermal and nonthermal bands, with their own unique observational features (Zimovets et al. 2021). However, it is not clear whether one of those mechanisms could explain the observed period ratio.

Analysis and interpretation of QPPs in Sections 3–5 were supported by the Russian Science Foundation grant No. 21-12-00195. D.Y.K. and V.M.N. acknowledge support from the STFC consolidated grant ST/T000252/1. V.M.N. was supported by the Russian Foundation for Basic Research grant No. 18-29-21016. D.Y.K. and A.A.K. acknowledge support from the Ministry of Science and Higher Education of the Russian Federation.

ORCID iDs

Dmitrii Y. Kolotkov <https://orcid.org/0000-0002-0687-6172>
 Valery M. Nakariakov <https://orcid.org/0000-0001-6423-8286>

Alexey A. Kuznetsov <https://orcid.org/0000-0001-8644-8372>

References

- Alfvén, H., & Carlqvist, P. 1967, *SoPh*, **1**, 220
- Anfinogentov, S., Nakariakov, V. M., Mathioudakis, M., Van Doorsselaere, T., & Kowalski, A. F. 2013, *ApJ*, **773**, 156
- Benz, A. O. 2017, *LRSP*, **14**, 2
- Benz, A. O., & Güdel, M. 2010, *ARA&A*, **48**, 241
- Borucki, W. J., Koch, D., Basri, G., et al. 2010, *Sci*, **327**, 977
- Broomhall, A.-M., Davenport, J. R. A., Hayes, L. A., et al. 2019b, *ApJS*, **244**, 44
- Broomhall, A. M., Thomas, A. E. L., Pugh, C. E., Pye, J. P., & Rosen, S. R. 2019a, *A&A*, **629**, A147
- Cho, I. H., Cho, K. S., Nakariakov, V. M., Kim, S., & Kumar, P. 2016, *ApJ*, **830**, 110
- Chorley, N., Hnat, B., Nakariakov, V. M., Inglis, A. R., & Bakunina, I. A. 2010, *A&A*, **513**, A27
- Doyle, J. G., Shetye, J., Antonova, A. E., et al. 2018, *MNRAS*, **475**, 2842
- Fletcher, L., Dennis, B. R., Hudson, H. S., et al. 2011, *SSRv*, **159**, 19
- Gaia Collaboration 2018, *yCat*, I/345
- Guarcello, M. G., Micela, G., Sciortino, S., et al. 2019, *A&A*, **622**, A210
- Güdel, M. 2004, *A&ARv*, **12**, 71
- Huang, N. E., Shen, Z., Long, S. R., et al. 1998, *RSPSA*, **454**, 903
- Ilin, E., Poppenhaeger, K., Schmidt, S. J., et al. 2021, *MNRAS*, **507**, 1723
- Inglis, A. R., Zimovets, I. V., Dennis, B. R., et al. 2011, *A&A*, **530**, A47
- Jansen, F., Lumb, D., Altieri, B., et al. 2001, *A&A*, **365**, L1
- Khodachenko, M. L., Zaitsev, V. V., Kislyakov, A. G., & Stepanov, A. V. 2009, *SSRv*, **149**, 83
- Kupriyanova, E., Kolotkov, D., Nakariakov, V., & Kaufman, A. 2020, *STP*, **6**, 3
- Kuznetsov, A. A., & Kolotkov, D. Y. 2021, *ApJ*, **912**, 81
- Li, B., Antolin, P., Guo, M. Z., et al. 2020, *SSRv*, **216**, 136
- Maehara, H., Shibayama, T., Notsu, S., et al. 2012, *Natur*, **485**, 478
- Mathioudakis, M., Bloomfield, D. S., Jess, D. B., Dhillon, V. S., & Marsh, T. R. 2006, *A&A*, **456**, 323
- McLaughlin, J. A., Nakariakov, V. M., Dominique, M., Jelínek, P., & Takasao, S. 2018, *SSRv*, **214**, 45
- McQuillan, A., Mazeh, T., & Aigrain, S. 2014, *ApJS*, **211**, 24
- Mitra-Kraev, U., Harra, L. K., Williams, D. R., & Kraev, E. 2005, *A&A*, **436**, 1041
- Monsignori Fossi, B. C., Landini, M., Del Zanna, G., & Bowyer, S. 1996, *ApJ*, **466**, 427
- Nakariakov, V. M., Hornsey, C., & Melnikov, V. F. 2012, *ApJ*, **761**, 134
- Nakariakov, V. M., & Kolotkov, D. Y. 2020, *ARA&A*, **58**, 441
- Nakariakov, V. M., Kolotkov, D. Y., Kupriyanova, E. G., et al. 2019, *PPCF*, **61**, 014024
- Nakariakov, V. M., & Melnikov, V. F. 2009, *SSRv*, **149**, 119
- Neupert, W. M. 1968, *ApJL*, **153**, L59
- Pizzocaro, D., Stelzer, B., Poretti, E., et al. 2019, *A&A*, **628**, A41
- Pugh, C. E., Armstrong, D. J., Nakariakov, V. M., & Broomhall, A. M. 2016, *MNRAS*, **459**, 3659
- Pugh, C. E., Broomhall, A. M., & Nakariakov, V. M. 2017, *A&A*, **602**, A47
- Pugh, C. E., Nakariakov, V. M., & Broomhall, A. M. 2015, *ApJL*, **813**, L5
- Ramsay, G., Kolotkov, D., Doyle, J. G., & Doyle, L. 2021, *SoPh*, **296**, 162
- Rosen, S. R., Webb, N. A., Watson, M. G., et al. 2016, *A&A*, **590**, A1
- Schrijver, C. J. 2011, in ASP Conf. Ser. 448, 16th Cambridge Workshop on Cool Stars, Stellar Systems, and the Sun, ed. C. Johns-Krull, M. K. Browning, & A. A. West (San Francisco, CA: ASP), 231
- Shibata, K., & Magara, T. 2011, *LRSP*, **8**, 6
- Stepanov, A. V., Kliem, B., Zaitsev, V. V., et al. 2001, *A&A*, **374**, 1072
- Tan, B., Yu, Z., Huang, J., Tan, C., & Zhang, Y. 2016, *ApJ*, **833**, 206
- Vaughan, S. 2005, *A&A*, **431**, 391
- Zaitsev, V. V., & Stepanov, A. V. 2008, *PhyU*, **51**, 1123
- Zaitsev, V. V., Stepanov, A. V., Urpo, S., & Pohjolainen, S. 1998, *A&A*, **337**, 887
- Zhilyaev, B. E., Romanyuk, Y. O., Verlyuk, I. A., et al. 2000, *A&A*, **364**, 641
- Zimovets, I. V., McLaughlin, J. A., Srivastava, A. K., et al. 2021, *SSRv*, **217**, 66